The versatile synthesis of polyhedron core/shell/shell $Cd_{0.1}Zn_{0.9}Se/Cd_xZn_{1-x}S/ZnS$ quantum dots

Liudmila Loghina
Center of Materials and Nanotechnologies, Faculty of Chemical Technology
University of Pardubice
Pardubice, Czech Republic
Liudmila.Loghina@upce.cz

Maksym Chylii
Center of Materials and Nanotechnologies, Faculty of Chemical Technology
University of Pardubice
Pardubice, Czech Republic
Maksym.Chylii@upce.cz

Anastasia Kaderavkova
Center of Materials and Nanotechnologies, Faculty of Chemical Technology
University of Pardubice
Pardubice, Czech Republic
Anastasia.Kaderavkova@upce.cz

Jakub Houdek
Center of Materials and Nanotechnologies, Faculty of Chemical Technology
University of Pardubice
Pardubice, Czech Republic
st34492@student.upce.cz

Miroslav Vlcek
Center of Materials and Nanotechnologies, Faculty of Chemical Technology
University of Pardubice
Pardubice, Czech Republic
Miroslav.Vlcek@upce.cz

***Abstract*—One of the most effective strategies for reducing the surface defects in nanocrystals is the shell growth on the already formed cores. This approach provides not only an increase in the photoluminescence quantum yield (PL QY) but also prevents the diffusion of cations and anions from the core material. Gram scale synthesis of the green-emitting core (10 g) was performed by interaction of highly reactive substituted selenourea ((*Z*)-N-(octadec-9-enyl)morpholine-4-carboselenoamide) with the cadmium and zinc linoleates mixture at 240 °C. Verification of the shell growth method based on the volume ratios of the core and the core with a shell led to the creation of a series of core/shell/shell $Cd_{0.1}Zn_{0.9}Se/Cd_xZn_{1-x}S/ZnS$ (x = 0.1; 0.25; 0.4; 0.6; 0.75) quantum dots (QDs). Deposition of the first shell ((*Z*)-1-(octadec-9-enyl)-3-phenylthiourea) of $Cd_xZn_{1-x}S$ composition with a thickness of 2 monolayers (MLs) (epitaxial growth) resulted in blue (x = 0.1 and 0.25) and red (x = 0.4; 0.6 and 0.75) shifts in emission bands and an increase in PL QY (up to 71 %). The deposition of the second ZnS shell (2 MLs), the same for all compositions, was not epitaxial to the core, which brought a change in shape but did not affect the optical properties of the material. The analysis of $Cd_{0.1}Zn_{0.9}Se/Cd_xZn_{1-x}S/ZnS$ core/shell/shell by EDS, XPS, and XRD methods, confirmed the accordance of the initial ratios with the given compositions and sizes.**

***Keywords*—core/shell/shell quantum dots, methodology, substituted thiourea, substituted selenourea, photoluminescence**

I. Introduction

The demand for the unique properties of nanomaterials leads to the expansion of methods for their preparation, in particular, to the search for commercially available starting reagents, reducing environmental damage, and optimizing the yield of the product without loss of their properties [1, 2]. The chalcogenide quantum dots (QDs) are the most widely used in the fabrication of light-emitting diodes [3, 4], radiation detectors [5, 6], solar cells [7, 8], as biological labels [9, 10], *etc*.

The kinetics of nanocrystal formation directly depends on the structure of the starting materials [11]. And, despite the widespread use of the corresponding phosphines as sources of chalcogens [12], substituted thio- and selenoureas also proved to be highly reactive precursors [13], which make it possible to create homogeneous and highly photoluminescent nanomaterials. It should be emphasized that the product conversion, in the case of such sources of sulfur and selenium, is close to 100 % [14].

The deposition of a zinc sulfide shell onto the $Cd_{0.25}Zn_{0.75}Se$ core with the participation of disubstituted thiourea was for the first time performed by our group [14]. The development of this method has led to the creation of the polyhedron $Cd_{0.1}Zn_{0.9}Se/Cd_xZn_{1-x}S/ZnS$ (x = 0.1; 0.25; 0.4; 0.6; 0.75) core/shell/shell QDs series. The controlled supply of the shell material to the already formed core, as well as the developed method for calculating all involved components, together with the high conversion of the final nanomaterial, make it possible to transfer this study to the industrial gram-scale synthesis of the highly photoluminescent nanomaterials.

II. Experiment

A. Chemicals

Selenium (Se, 99.9 %), phenyl isothiocyanate (PhNCS, 98 %), morpholine (99 %), aniline ($PhNH_2$, 99 %), cadmium oxide (CdO, 99.9 %), zinc oxide (ZnO, 99 %), 1-octadecene (ODE, technical grade, 90 %), linoleic acid (LA, technical grade 60-74 %), oleylamine (OAm, technical grade, 70 %), chloroform-d ($CDCl_3$, 99.8 atom % D) and silica gel (high-purity grade, pore size 60 Å, 230-400 mesh particle size) were purchased from Sigma-Aldrich and used without further purification. ((*Z*)-N-(octadec-9-enyl)morpholine-4-carboselenoamide (*SU*) and (*Z*)-1-(octadec-9-enyl)-3-phenylthiourea (*TU*) were synthesized in our laboratory previously [14]. Syntheses of QDs were carried out using standard Schlenk techniques under an inert atmosphere.

B. Synthesis of the $Cd_{0.1}Zn_{0.9}Se$ core

Synthesis of $Cd_{0.1}Zn_{0.9}Se$ QDs was conducted similarly to that published earlier [14] with recalculation of the initial

components amounts to obtain the corresponding composition. Briefly, a mixture of Cd and Zn linoleates was carried out from CdO (0.81 g, 0.00632 mol), ZnO (4.62 g, 0.0568 mol), LA (53.3 g, 0.19 mol) and 160 ml ODE at 150 °C for 1 hour. A solution of *SU* (28.0 g, 0.0632 mol) in the mixture of OAm (16.9 g, 0.0632 mol) and 20 ml ODE was made in a separate flask with stirring at 50 °C. To the mixture of linoleates at 240 °C in an argon atmosphere, a freshly prepared *SU* solution was added in one portion. Nucleation was accompanied by an immediate orange color of the reaction mixture. The growth of QDs was continued for 20 minutes without changing the temperature. The isolation and purification of $Cd_{0.1}Zn_{0.9}Se$ QDs were performed from a spontaneously cooled colloidal solution with a mixture of chloroform and acetone. After drying in a vacuum, the mass of the product was 10.8 g (calc. 9.4 g). The excess in the mass of the product was due to the organic tails of the nanocrystal's protective shell.

C. *Synthesis of the $Cd_{0.1}Zn_{0.9}Se/Cd_xZn_{1-x}S$ core/shell QDs*

The calculation of the materials required for the deposition of 2 MLs of the shell was conducted according to the scheme published earlier [14]. $Cd_{0.1}Zn_{0.9}Se$ QDs (core, 1.0 g) were introduced into a freshly prepared solution of cadmium and zinc linoleates with a given ratio and a total volume of 25 ml. To deposit 2 MLs of the $Cd_xZn_{1-x}S$ shell, 65.6 % (x = 0.1), 68.8 % (x = 0.25), 71.3 % (x = 0.4), 76.9 % (x = 0.6) and 80.5 % (x = 0.75) of the shell material from the mass of core were required. The introduction of a solution of *TU* in a similar amount of OAm and ODE, with a total volume of 10 ml, was performed at 240 °C in portions of 1 ml every 2 minutes. After the introduction of *TU*, the growth continued for another 10 minutes. The process of isolation and purification was described above (II.B). The mass of obtained $Cd_{0.1}Zn_{0.9}Se/Cd_xZn_{1-x}S$ QDs was 1.6 – 1.8 g.

D. *Synthesis of the $Cd_{0.1}Zn_{0.9}Se/Cd_xZn_{1-x}S/ZnS$ core/shell/shell QDs*

The deposition of the second shell of the ZnS composition was conducted similarly to that described above with the corresponding calculations of the shell materials. $Cd_{0.1}Zn_{0.9}Se$/ $Cd_xZn_{1-x}S$ QDs (1.0 g) were introduced into a freshly prepared solution of zinc linoleate in ODE with a given ratio and a total volume of 25 ml. To deposit 2 MLs of a ZnS shell, 134.7 % (x = 0.1), 136.6 % (x = 0.25), 133.6 % (x = 0.4), 135.8 % (x = 0.6) and 136.1 % (x = 0.75) of the shell material from the mass of core were required. The mass of the core/shell/shell $Cd_{0.1}Zn_{0.9}Se/Cd_xZn_{1-x}S/ZnS$ QDs was 2.1 – 2.3 g.

III. RESULTS AND DISCUSSIONS

A. *The $Cd_{0.1}Zn_{0.9}Se/Cd_xZn_{1-x}S/ZnS$ core/shell/shell QDs synthesis*

The controlled growth of nanocrystals is ensured by the controlled introduction of molecular components into the growth medium, followed by their saturation, nucleation, and growth. In turn, the regulated flow of molecular chalcogenides is guaranteed by the nature of the initial components and, accordingly, their interaction rate. Therefore, the higher the reactivity of the chalcogen sources, the higher the conversion and the narrower nanocrystal size distribution. Substituted thio- and selenoureas, being highly reactive [15] (almost instantly at relatively high temperatures) form complexes with metal carboxylates [16]. These complexes decompose with the release of the corresponding sulfides and selenides, creating a short but stable saturation of the medium with the building blocks of nanocrystals.

The growth of a relatively thin shell (2 MLs) was carried out by the successive introduction of the calculated amount of substituted thiourea dissolved in a mixture of OAm and ODE into the mixture of the cationic component and dispersed cores (Fig. 1). The calculation of the required amounts of shell material was based on the ratio of the known core volume to the desired core/shell volume QDs [14]. This method was applied for the first time on the presented material $Cd_{0.1}Zn_{0.9}Se/Cd_xZn_{1-x}S/ZnS$ core/shell/shell QDs.

B. *The crystalline structure and morphology of the $Cd_{0.1}Zn_{0.9}Se/Cd_xZn_{1-x}S/ZnS$ core/shell/shell QDs*

X-Ray diffraction patterns (XRD) were registered using PANalytical EMPYREAN powder X-Ray diffractometer (ALMELO, Netherlands) with Cu-Kα radiation (λ = 1.5418 Å). The data from $Cd_{0.1}Zn_{0.9}Se/Cd_xZn_{1-x}S/ZnS$ core/shell/shell QDs were obtained across a 2θ range of 15 - 100° with a step size of 0.05° (Fig. 2a). Standard diffraction lines of cubic $Cd_{0.1}Zn_{0.9}Se$ (ICSD:192338), CdS (ICSD:181739) and ZnS (ICSD:53943) are drawn for comparison. $Cd_xZn_{1-x}S$ shells grow epitaxially to the core in the same face-centered cubic phase with the space group F-43*m*. With an increase of the Cd content in the shell, all three diffraction peaks shift towards smaller angles, reaching a position corresponding to cubic CdS.

Upon growth of the second ZnS shell (2 MLs), a noticeable superposition of the second group of signals corresponding to the cubic ZnS structure was observed. The

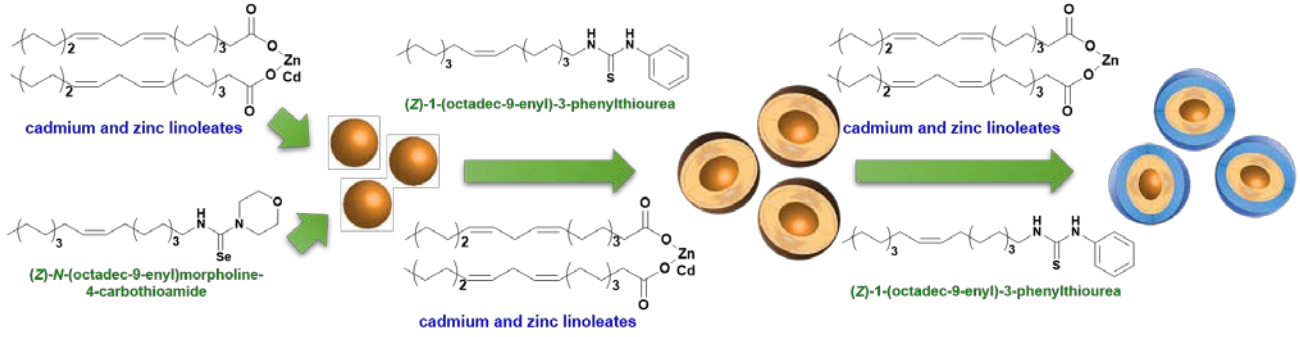

Fig. 1. The schematic illustration of $Cd_{0.1}Zn_{0.9}Se/Cd_xZn_{1-x}S/ZnS$ core/shell/shell QDs synthesis.

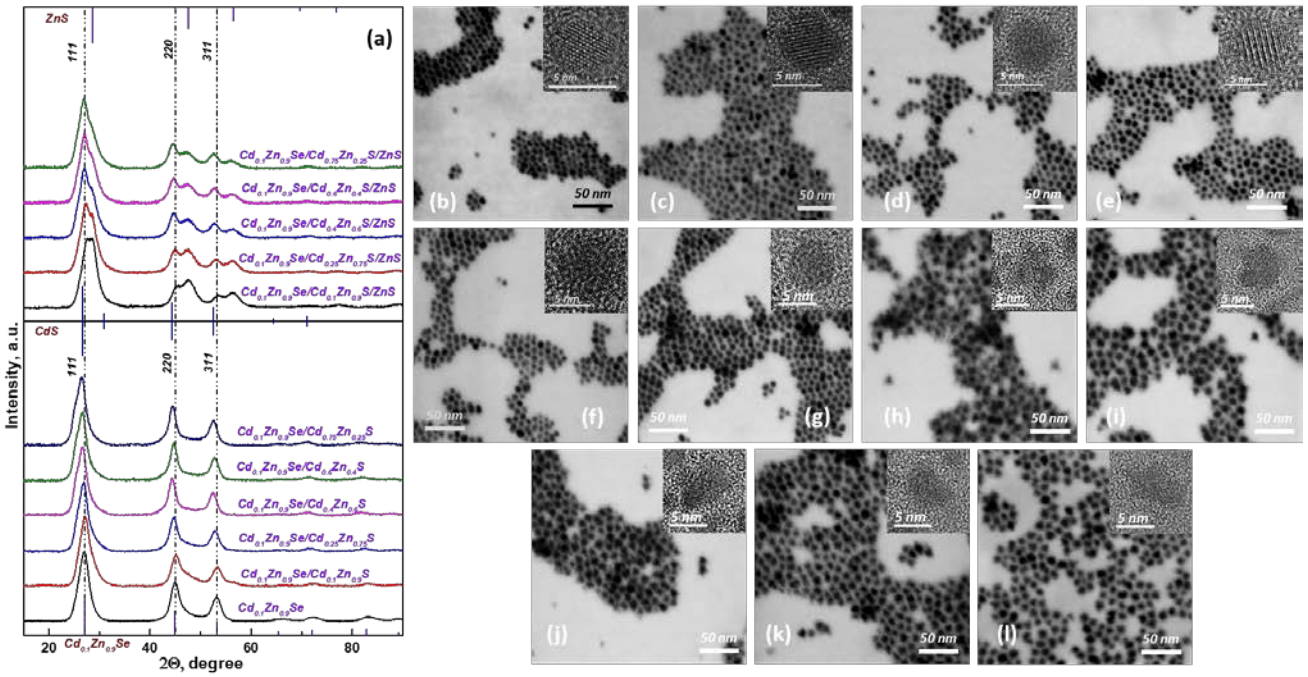

Fig. 2. XRD patterns of $Cd_{0.1}Zn_{0.9}Se/Cd_xZn_{1-x}S/ZnS$ core/shell/shell QDs; STEM and HR TEM (inset) images of $Cd_{0.1}Zn_{0.9}Se$ core (b); $Cd_{0.1}Zn_{0.9}Se/Cd_xZn_{1-x}S$ core/shell QDs, where x = 0.1 (c), x = 0.25 (d), x = 0.4 (e), x = 0.6 (f), x = 0.75 (g) and $Cd_{0.1}Zn_{0.9}Se/Cd_xZn_{1-x}S/ZnS$ core/shell/shell QDs, where x = 0.1 (h), x = 0.25 (i), x = 0.4 (j), x = 0.6 (k), x = 0.75 (l).

intensity of these signals respective to the signals of the core correlates with the corresponding STEM and HR TEM images, *i.e.* the proportion of the non-epitaxially growing shell decreases with an increase of the Cd content in the first shell. The average crystalline size was calculated according to Debye Scherrer's equation [17] and STEM images. According to the obtained empirical data, the QD size (Table 1) at all stages of the shell growth corresponds to the theoretical one with an error of 0.2 nm. To visualize the structure of $Cd_{0.1}Zn_{0.9}Se/Cd_xZn_{1-x}S/ZnS$ core/shell/shell QDs with sufficient atomic resolution and contrast, a high-resolution TEM imaging (HR TEM) was performed (Fig. 2b-l inset).

The surface chemical composition was determined by X-Ray photoelectron spectroscopy (XPS, ESCA 2SR, Scienta-Omicron) using a monochromatic Al Kα source (1486.6 eV). The binding energy scale was referenced to adventitious carbon (284.8 eV). The presence of C, O, Cd, Zn, Se, and S were confirmed through the survey spectra of $Cd_{0.1}Zn_{0.9}Se/Cd_{0.6}Zn_{0.4}S/ZnS$ QDs displayed in Figure 3a.

The changes in the intensity of the Cd and Zn signals of the core sample with respect to the core/shell and core/shell/shell samples were observed. It was due to the fact that by changing the first shell's composition, a greater amount of Cd was detected. The oxidation states of cations (Cd^{2+} and Zn^{2+}) were confirmed by high resolution spectra (Fig. 3b, c), where their spin-orbit splitting Cd $3d_{5/2}$ / Cd $3d_{3/2}$ signals are centered at 404.8 eV / 411.5 eV and Zn $2p_{3/2}$ / Zn $2p_{1/2}$ doublet appears at 1021.8 eV / 1044.8 eV. A strong overlapping between the S *2p* and Se *3p* signals was observed (Fig. 3e). The spectrum was deconvoluted with four components, the most intense pair corresponds to the spin-orbit splitting of S $2p_{3/2}$ / S $2p_{1/2}$, centered at 161.7 eV / 162. 9 eV, which is designated to S^{2-} species, related to Zn-S bond from the first and second shells.

Energy dispersion X-Ray microanalysis of all synthesized nanopowders (EDS) was carried out using scanning electron microscope LYRA 3 (Tescan, Czech Republic) equipped with EDS analyzer Aztec X-Max 20 (Oxford Instruments) at acceleration voltage 20 kV. The elemental analysis data (Cd, Zn, Se, S) of the synthesized QDs correspond to the nominal composition with a minimum error. Also, carbon and trace amounts of oxygen and nitrogen were found in the EDS spectra, corresponding to metal linoleates and oleylamine that build up the protective shell of QDs.

C. The optical properties of the $Cd_{0.1}Zn_{0.9}Se/Cd_xZn_{1-x}S/ZnS$ core/shell/shell QDs

The QDs optical properties were measured using UV-3600 (Shimadzu) spectrometer to get UV-Vis absorbance (ABS) spectra in the spectral range of 200 - 700 nm (Fig. 4a) and Fluorometer PTI QuantaMaster 400 (Horiba Scientific) to obtain photoluminescence (PL) data in the spectral range of 250 - 850 nm (Fig. 4b) using xenon lamp (75 W) as the excitation source. A change in the positions of the emission and the first exciton absorbance maxima in ABS and PL spectra of $Cd_{0.1}Zn_{0.9}Se/Cd_xZn_{1-x}S$ core/shell QDs was detected. Specifically, with a modification of Cd content in the shell, blue (x = 0.1, 0.25) and red (x = 0.4, 0.6, 0.75) shifts were observed. This phenomenon is associated with the diffusion of Cd from the cationic component presented in the growth medium into the core, followed by the formation of an intermediate layer that changes the band gap of the material [18]. The growth of the first shell occurred epitaxially to the core, which led to a change in the intensity of the PL signal of $Cd_{0.1}Zn_{0.9}Se/Cd_xZn_{1-x}S$ core/shell QDs and a sharp increase in PL QY (Table 1). The growth of the second shell (ZnS) proceeded non-epitaxially and had no significant effect on the emission of core/shell/shell QDs.

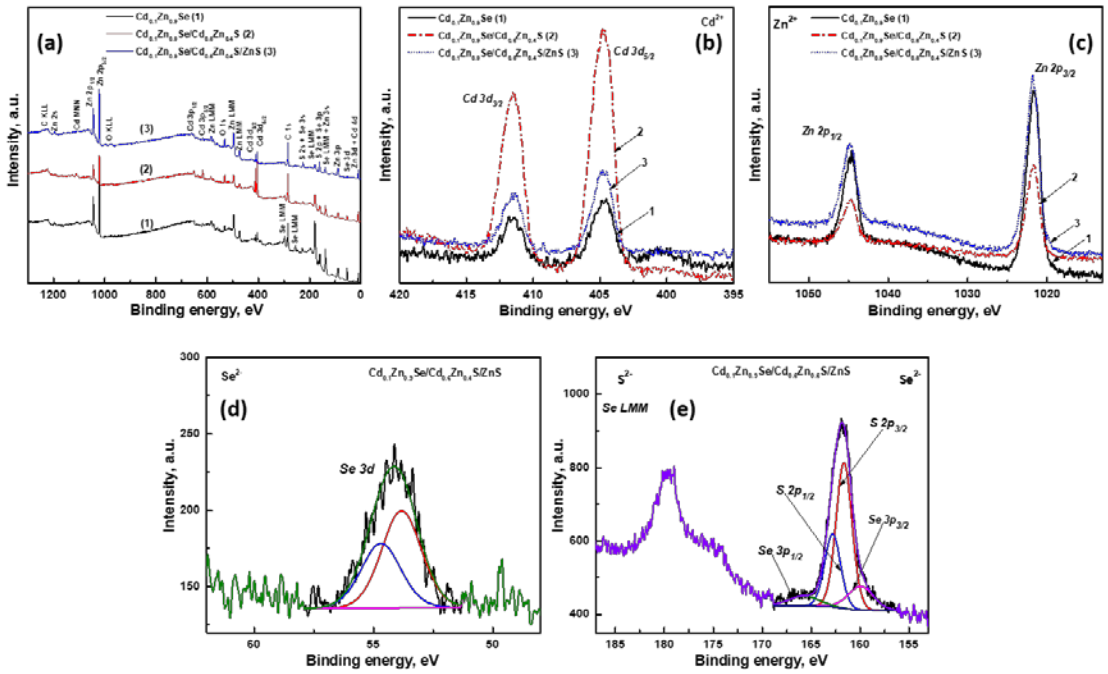

Fig. 3. XPS survey spectra of $Cd_{0.1}Zn_{0.9}Se/Cd_{0.6}Zn_{0.4}S/ZnS$ core/shell/shell QDs (a); chemical state analysis of Cd *3d* (b), Zn *2p* (c), and Se *3d* (d) and strong overlap between S *2p* and Se *3p* (e).

There is only some broadening of the PL spectra and a slight rising in their PL QY value. These changes are clearly visible from the QDs comparison spectra of absorbance and emission of the core, the core with the first shell (1) and the core with the second shell (2) (Fig. 4f-i).

The growth of the first and second shells led to the significant changes in their photoluminescence decay kinetics curves. The PL lifetime measurements were performed using TCSPC accessories for Fluorometer PTI QuantaMaster 400 with 456 nm light pulse excitation and the pulse half-width 0.8 ns produced by NanoLED 455 (Horiba Scientific). Photoluminescence decay kinetics curves were analyzed by PTI Felix GX software. Curve fitting and calculation of the average decay time were carried out similarly to the previously published results [14]. During the epitaxial growth of the shell, healing of surface defects and a decrease in the probability of nonradiative relaxation of charge carriers occurred [19]. This leads to a flattening of the kinetic curves (Fig. 4c), a rising in PL QY and the average

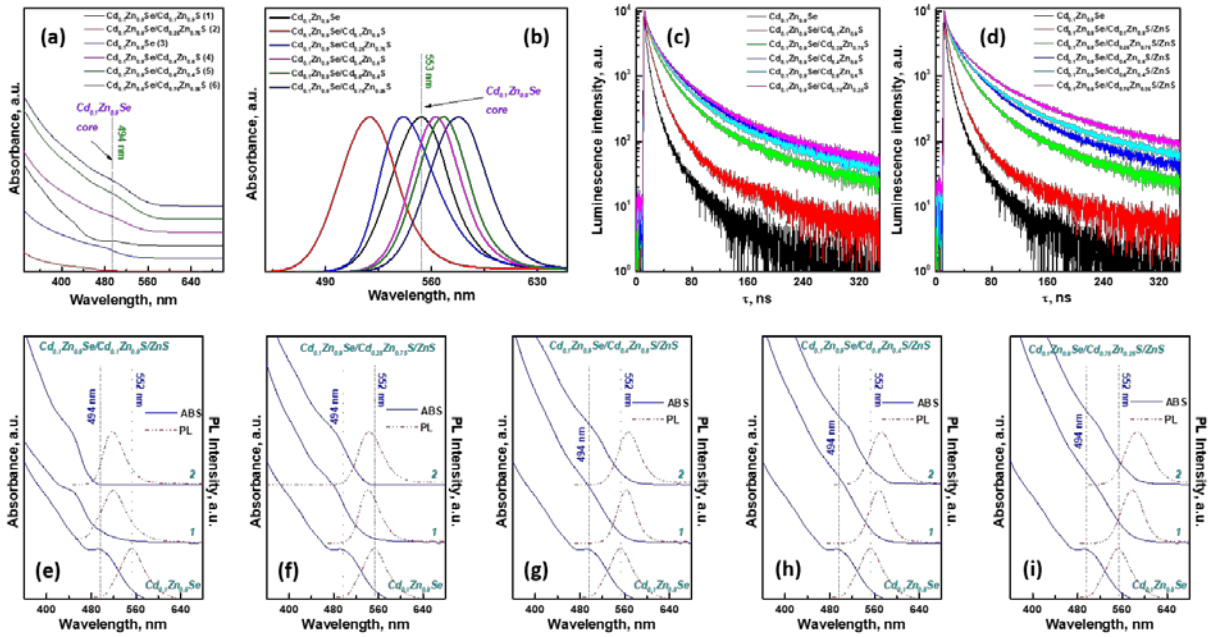

Fig. 4. ABS spectra (a) and normalized PL emission spectra (b) of $Cd_{0.1}Zn_{0.9}Se/Cd_xZn_{1-x}S$ core/shell QDs; PL decay kinetic curves of $Cd_{0.1}Zn_{0.9}Se/Cd_xZn_{1-x}S$ core/shell QDs (c) and $Cd_{0.1}Zn_{0.9}Se/Cd_xZn_{1-x}S/ZnS$ core/shell/shell QDs (d); comparison of ABS (blue solid lines) and PL emission (red dashed lines) of $Cd_{0.1}Zn_{0.9}Se/Cd_xZn_{1-x}S/ZnS$ core/shell/shell QDs, where x = 0.1 (e), x = 0.25 (f), x = 0.4 (g), x = 0.6 (h), x = 0.75 (i).

PL decay time (Table 1). With non-epitaxial growth, new defects may appear, which usually bring the opposite effects. In our case, the addition of the ZnS shell had no negative effect on the PL decay kinetics curves (Fig. 4d). Consequently, the non-epitaxial growth of the second shell did not bring a surface degradation, and the ZnS shell does not participate in the photoluminescence of core/shell/shell QDs but acts mainly as a protective shell that prevents the removal of cations and anions from the core material.

TABLE I. SIZE AND OPTICAL PROPERTIES OF $Cd_{0.1}Zn_{0.9}Se/Cd_xZn_{1-x}S/ZnS$ CORE/SHELL/SHELL QDS. PEAK MAXIMUM IN THE ABS SPECTRA (Λ_{ABS}), EXCITATION WAVELENGTH (Λ_{EXC}), PEAK MAXIMUM IN THE PL SPECTRA (Λ_{EM}), STOKES SHIFT, PL QY, AVERAGE PL LIFETIME (T_{AVG}).

Composition	**Size, nm**	**Optical parameters**					
		λ_{ABS}, nm	***λ_{exc}, nm***	***λ_{em}, nm***	***Stokes shift, nm***	***PL QY, %***	***τ_{avg}, ns***
$Cd_{0.1}Zn_{0.9}Se$	5.58	494	410	552	58	28	8.26
$Cd_{0.1}Zn_{0.9}Se/Cd_{0.1}Zn_{0.9}S$	6.72	448	410	519	71	49	13.91
$Cd_{0.1}Zn_{0.9}Se/Cd_{0.25}Zn_{0.75}S$	6.81	484	410	542	58	51	29.56
$Cd_{0.1}Zn_{0.9}Se/Cd_{0.4}Zn_{0.6}S$	6.79	500	410	563	63	55	38.13
$Cd_{0.1}Zn_{0.9}Se/Cd_{0.6}Zn_{0.4}S$	6.92	511	460	569	58	61	35.95
$Cd_{0.1}Zn_{0.9}Se/Cd_{0.75}Zn_{0.25}S$	6.98	518	480	578	60	63	41.46
$Cd_{0.1}Zn_{0.9}Se/Cd_{0.1}Zn_{0.9}S/ZnS$	7.91	446	420	519	73	50	13.22
$Cd_{0.1}Zn_{0.9}Se/Cd_{0.25}Zn_{0.75}S/ZnS$	7.99	483	460	544	61	54	34.44
$Cd_{0.1}Zn_{0.9}Se/Cd_{0.4}Zn_{0.6}S/ZnS$	8.07	507	460	567	50	61	45.25
$Cd_{0.1}Zn_{0.9}Se/Cd_{0.6}Zn_{0.4}S/ZnS$	8.12	518	480	572	54	68	44.99
$Cd_{0.1}Zn_{0.9}Se/Cd_{0.75}Zn_{0.25}S/ZnS$	8.24	523	480	586	63	71	53.41

IV. CONCLUSIONS

To conclude, we have presented a new method for the preparation of the $Cd_{0.1}Zn_{0.9}Se/Cd_xZn_{1-x}S/ZnS$ core/shell/shell QDs using available and highly reactive chalcogen sources. The interaction of substituted selenourea ((*Z*)-N-(octadec-9-enyl)morpholine-4-carboselenoamide) with cadmium and zinc linoleates was adapted to conduct the gram-scale synthesis of the core. It was demonstrated that the quantitative calculation of shell materials for the core of a known volume with the use of substituted thiourea ((*Z*)-1-(octadec-9-enyl)-3-phenylthiourea) can be successfully applied to the synthesis of multilayer nanostructures. Epitaxially growing 2 MLs of the $Cd_xZn_{1-x}S$ composition significantly increase PL QY (up to 71 %) due to the healing of surface defects. At the same time, the second shell of the ZnS composition protects the core against the Cd removal and does not distort the optical characteristics of core/shell/shell QDs. Prospects of this research development may affect the creation of highly photoluminescent nanomaterials with desired characteristics.

ACKNOWLEDGMENT

Authors appreciate the financial support from the project "High-sensitive and low-density materials based on polymeric nanocomposites" - NANOMAT (No. CZ.02.1.01/0.0/0.0/17_048/0007376) and grant LM2018103 from the Ministry of Education, Youth and Sports of the Czech Republic.

REFERENCES

[1] R. G. Chaudhuri and Santanu Paria, "Core/Shell Nanoparticles: Classes, Properties, Synthesis Mechanisms, Characterization, and Applications," Chem. Rev., vol. 112, pp. 2373–2433, December 2012.

[2] P. Reiss, M. Protie`re, and Liang Li, "Core/Shell Semiconductor Nanocrystals," Small, Vol. 5, Issue 2, pp. 154-168, January, 2009.

[3] T. Lee, D. Hahm, K. Kim, W. K. Bae, C. Lee, and J. Kwak, "Highly efficient and bright inverted top-emitting InP quantum dot light-emitting diodes introducing a hole-suppressing interlayer," Small, Vol. 15, Issue 50, p. 1905162, December, 2019.

Ministry of Education, Youth and Sports of the Czech Republic.

[4] D.-W. Shin, Y.-H. Suh, S. Lee, B. Hou, S. D. Han, Y. Cho, X.-B. Fan, S. Y. Bang, S. Zhan, J. Yang, H. W. Choi, S. J., F. C. Mocanu, H. Lee, L. Occhipinti, Y. T. Chun, G. Amaratunga, and J. M. Kim, "Waterproof flexible InP@ZnSeS quantum dot light-emitting diode," Adv.OpticalMater., Vol. 8, Issue 6, p. 1901362, March 2020.

[5] C. Liu, Z. Li, T. J. Hajagos, D. Kishpaugh, D. Y. Chen, and Q. Pei, "Transparent ultra-high-loading quantum dot/polymer nanocomposite monolith for gamma scintillation," ACS Nano, Vol. 11, Issue 6, pp. 6422–6430, May 2017.

[6] C. L. Wang, L. Gou, J. M. Zaleski, and D. L. Friesel, "ZnS quantum dot based nanocomposite scintillators for thermal neutron detection," Nuclear Instruments and Methods in Physics Research A, Vol. 622, pp. 186–190, October 2010.

[7] P. Singh, R. Gautam, S. Sharma, S. Kumari, and A.S. Verma, "Simulated solar cell device of $CuGaSe_2$ by using CdS, ZnS and ZnSe buffer layers," Materials Science in Semiconductor Processing, Vol. 42, pp. 288–302, February 2016.

[8] M.M. Islam, S. Ishizuka, A. Yamada, K. Sakurai, S. Niki, T. Sakurai, and K. Akimoto, "CIGS solar cell with MBE-grown ZnS buffer layer," Solar Energy Materials & Solar Cellsm, Vol. 93, pp. 970–972, June 2009.

[9] O. Adegoke, M.-W. Seo, T. Kato, S. Kawahito, and E. Y. Park, "Gradient band gap engineered alloyed quaternary/ternary CdZnSeS/ZnSeS quantum dots: an ultrasensitive fluorescence reporter in a conjugated molecular beacon system for the biosensing of influenza virus RNA," J. Mater. Chem. B, Vol. 4, p. 1489, January 2016.

[10] A. A. P. Mansur, H. S. Mansur, R. L. Mansur, F. G. de Carvalho, and S. M. Carvalho, "Bioengineered II–VI semiconductor quantum dot-carboxymethylcellulose nanoconjugates as multifunctional fluorescent nanoprobes for bioimaging live cells," Spectrochimica Acta Part A: Molecular and Biomolecular Spectroscopy, Vol. 189 pp. 393–404, January 2018.

[11] L. S. Hamachi, I. Jen-La Plante, A. C. Coryell, J. De Roo, and J. S. Owen, "Kinetic control over CdS nanocrystal nucleation using a library of thiocarbonates, thiocarbamates, and thioureas," Chem. Mater., Vol. 29, pp. 8711–8719, October 2017.

[12] R. García-Rodríguez, M. P. Hendricks, B. M. Cossairt, H. Liu, and J. S. Owen, "Conversion reactions of cadmium chalcogenide nanocrystal precursors," Chem. Mater., Vol. 25, pp. 1233−1249, February 2013.

[13] M. Chylii, L. Loghina, A. Kaderavkova, S. Slang, P. Svec, J. Rodriguez Pereira, B. Frumarova, D. Cizkova, A. Bezrouk, and M. Vlcek, "Enhanced optical properties of $ZnSe_xS_{1-x}$ and Mn-doped $ZnSe_xS_{1-x}$ QDs via non-toxic synthetic approach," Materials Chemistry and Physics, Vol. 284, p. 126060, May 2022.

[14] L. Loghina, M. Chylii, A. Kaderavkova, S. Slang, P. Svec, J. Rodriguez Pereira, B. Frumarova, M. Cieslar, and M. Vlcek, "Highly Efficient and Controllable Methodology of the $Cd_{0.25}Zn_{0.75}Se/ZnS$

Core/Shell Quantum Dots Synthesis," Nanomaterials, Vol. 11, p. 2616, September 2021.

[15] M. P. Hendricks, M. P. Campos, G. T. Cleveland, I. Jen-La Plante, and J. S. Owen, "A tunable library of substituted thiourea precursors to metal sulfide nanocrystals," Science, Vol. 348, Issue 6240, pp. 1226-1230, June 2015.

[16] L. Loghina, M. Grinco, A. Iakovleva, S. Slang, K. Palka, and M. Vlcek, "Mechanistic investigation of the sulfur precursor evolution in the synthesis of highly photoluminescent $Cd_{0.15}Zn_{0.85}S$ quantum dots," New J. Chem., Vol. 42, p. 14779, July 2018.

[17] J. I. Langford and A. J. C. Wilson, "Scherrer after sixty years: A survey and some new results in the determination of crystallite size," J. Appl. Cryst., Vol. 11, pp. 102-113, 1978.

[18] C. Li, W. Chen, D. Wu, D. Quan, Z. Zhou, J. Hao, J. Qin, Y. Li, Z. He, and K. Wang, "Large stokes shift and high efficiency luminescent solar concentrator incorporated with $CuInS_2$/ZnS quantum dots," Sci. Rep., Vol. 5, p. 17777, December 2016.

[19] A. N. Yadav, A. K. Singh, and Kedar Singh, "Synthesis, properties, and applications of II-VI semiconductor core/shell quantum dots," Springer, Lecture Notes in Nanoscale Science and Technology, Vol. 28, July 2020.